nature photonics

ARTICLES

https://doi.org/10.1038/s41566-021-00845-4

Check for updates

Quantum transport in fractal networks

Xiao-Yun Xu[1,2], Xiao-Wei Wang[1,2], Dan-Yang Chen[1], C. Morais Smith[3,4,5] ✉ and Xian-Min Jin[1,2,6] ✉

Fractals are fascinating, not only for their aesthetic appeal but also for allowing the investigation of physical properties in non-integer dimensions. In these unconventional systems, many intrinsic features might come into play, including the fractal dimension and the fractal geometry. Despite abundant theoretical studies, experiments in fractal networks remain elusive. Here we experimentally investigate quantum transport in fractal networks by performing continuous-time quantum walks in fractal photonic lattices. We unveil the transport properties through the photon evolution patterns, the mean square displacement and the Pólya number. Contrarily to classical fractals, we observe anomalous transport governed solely by the fractal dimension. In addition, the critical point at which there is a transition from normal to anomalous transport depends on the fractal geometry. Our experiment allows the verification of physical laws in a quantitative manner and reveals the transport dynamics in great detail, thus opening a path to the understanding of more complex quantum phenomena governed by fractality.

The word 'fractal' was coined by Mandelbrot for the description of complex structures that usually exhibit self-similarity and non-integer dimension[1,2]. Closely related to humankind, nature and science[3,4], fractality is not only widely embodied in common objects or scenarios, such as branching trees, fluctuations in the stock market or human heartbeat dynamics[5], but is also reflected in subtle physical properties and phenomena, such as an energy spectrum[6–8] or the growth of copper electrodeposits[9], thereby involving the fields of physiology[10,11], finance[12], quantum mechanics[13–15], optics[16–18] and so on. Inspired by these natural manifestations, the concept of the fractal has triggered novel designs of materials[19,20], photovoltaic and plasmonic devices[21–24], enriching the means of material property modification or of artificial device engineering.

The role of fractality has been extensively studied in the context of classical transport or diffusion by investigating classical random walk in fractal lattices[2,25,26]. Alexander and Orbach proposed that the spectral dimension and the Hausdorff dimension govern the classical diffusion in fractals[27,28]. Despite some disagreements on the nature of the diffusion laws, it is beyond doubt that fractality leads to anomalous diffusion, distinctive from regular lattices, in which the mean square displacement (MSD) scales linearly[29–31]. However, the interplay between quantum transport and fractality is still waiting for experimental exploration, despite abundant theoretical studies at non-integer dimensions[32–36] and pioneering experiments in integer-dimensional ordered[37–41], disordered[42–45] and non-Hermitian lattices[46]. Molecular synthesis[47–49], atomic manipulation techniques[50] and photorefractive materials[51] allow the construction of well-defined fractal structures, but these platforms are not prone to the detection of dynamical properties. Photonic lattices based on femtosecond-laser direct-writing techniques, on the other hand, are shown to be the ideal system to investigate quantum-transport dynamics, since they enable the precise design and fabrication of three-dimensional structures[52,53].

Here, we experimentally investigate quantum transport in fractal networks via continuous-time quantum walks of single photons, which are implemented on photonic lattices with identical fractal geometry but incremental propagation lengths. With the propagation length increasing, the evolution of photons at different moments is probed, visually revealing the transport dynamics. Based on the probability distribution of the evolution patterns, we calculate the MSD and the Pólya number[54] to characterize the transport process. Three kinds of fractals are experimentally realized to study the interplay between quantum transport and the geometrical or fractal features of the networks.

Results

Sierpiński gaskets, with a Hausdorff dimension or fractal dimension of 1.58, are representative deterministic fractals[34]. The first-generation of a Sierpiński gasket G(1) is constructed from a triangle by removing its central part, with three blue triangles left, see Fig. 1a. By applying the same operation on the remaining blue triangles, we acquire the subsequent generation G(2). Similarly, higher generations are produced through an iterative procedure, revealing the self-similarity of fractals and the fact that higher generations can be decomposed into lower ones. To map the fractal geometry into photonic lattices, we define lattice sites at the corners of the blue triangles. Figure 1b exhibits the cross-section of the photonic lattice for the fourth-generation Sierpiński gasket, which can be regarded as a composition of identical copies of G(1) (filled in blue and denoted by the arrow). The white circles represent lattice sites and the white lines connecting the circles correspond to the edges of the blue triangles. Note that the white lines are only used for identifying the fractal geometry and do not exist in the real photonic lattices.

According to the design, we fabricate the photonic lattice depicted in Fig. 1c in Corning Eagle XG glass through femtosecond-laser direct-writing techniques (see Methods). In light of the fact that the quantum dynamics of single photons in the lattices is equivalent to the spreading of a light beam[39], horizontally polarized photons (coming directly from a coherent light beam) with a wavelength of 810 nm are injected into the lattices to perform continuous-time quantum walks. Their evolution is governed by the Hamiltonian H of the system,

$$|(t)\rangle = \mathrm{e}^{-iHt}|(0)\rangle, \quad (1)$$

[1]Center for Integrated Quantum Information Technologies (IQIT), School of Physics and Astronomy and State Key Laboratory of Advanced Optical Communication Systems and Networks, Shanghai Jiao Tong University, Shanghai, China. [2]CAS Center for Excellence and Synergetic Innovation Center in Quantum Information and Quantum Physics, University of Science and Technology of China, Hefei, Anhui, China. [3]Institute for Theoretical Physics, Utrecht University, Utrecht, the Netherlands. [4]Tsung-Dao Lee Institute, Shanghai, China. [5]Wilczek Quantum Center, School of Physics and Astronomy, Shanghai Jiao Tong University, Shanghai, China. [6]TuringQ Co., Ltd., Shanghai, China. ✉e-mail: c.demoraissmith@uu.nl; xianmin.jin@sjtu.edu.cn

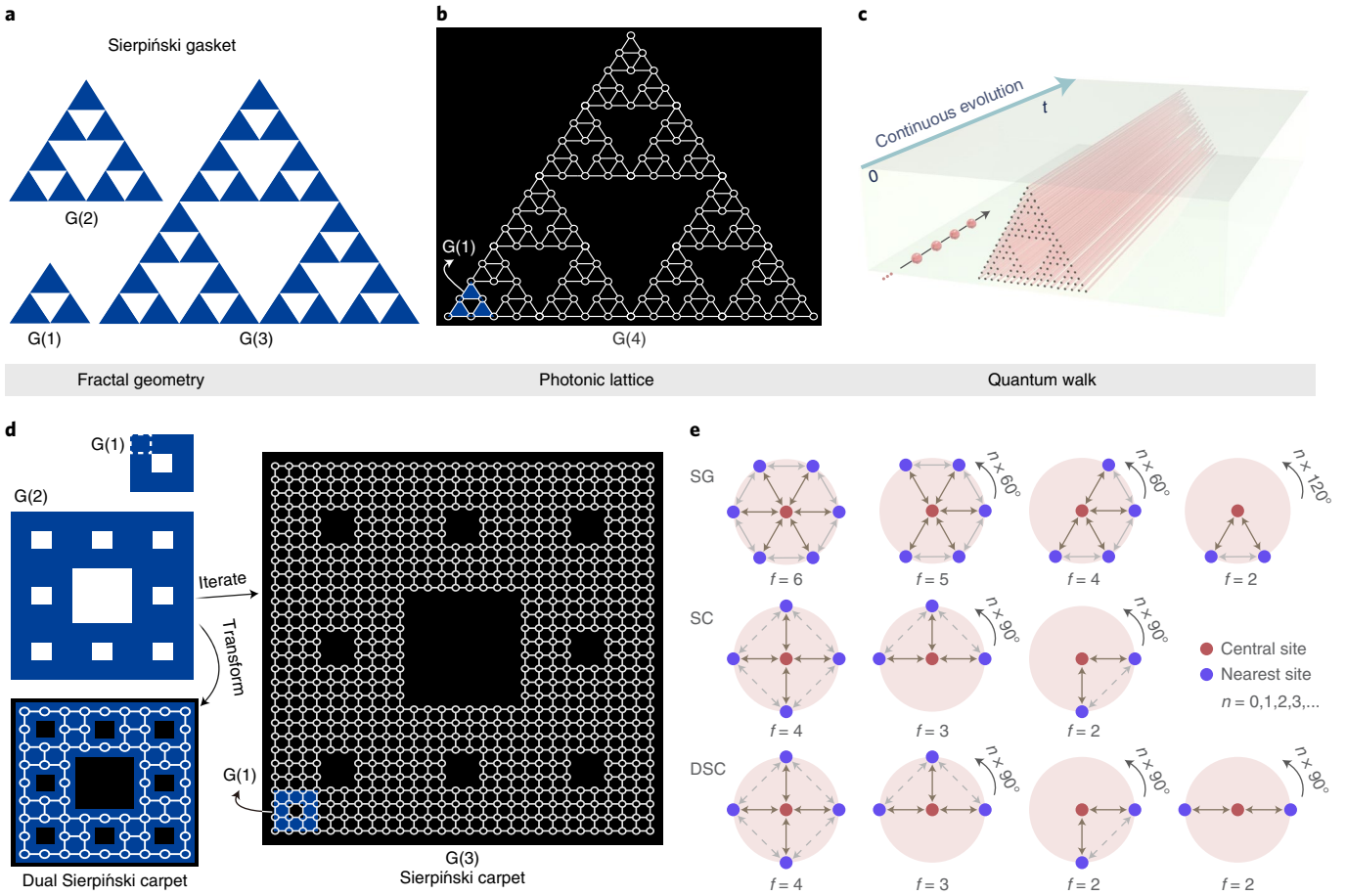

Fig. 1 | Geometry and connectivity analysis of the fractals, and implementation of quantum walks. a, The first-generation Sierpiński gasket G(1) is constructed by removing the central part of a triangle, leaving three blue triangles. Higher generations are produced through an iterative procedure. **b**, The photonic lattice for the fourth-generation Sierpiński gasket composed of G(1) filled with blue. The white circles correspond to the corners of blue triangles and represent lattice sites. The white lines linking the circles correspond to the edges of the blue triangles and are only used for identifying the fractal geometry. **c**, The photonic chip with an embedded lattice is used to implement continuous-time quantum walks by injecting photons. The evolution time t is related to the longitudinal length of the lattice. **d**, The first-generation Sierpiński carpet is constructed by removing the central part of a square, leaving eight blue squares, one of which is enclosed by the white dashed line. Higher generations are formed by iterating the procedure. The white circles correspond to the corners of the blue squares, representing lattice sites. The lattice for the dual Sierpiński carpet is obtained by replacing the blue squares in the second-generation Sierpiński carpet with lattice sites. **e**, Connectivity analysis. Only the nearest-neighbour sites are connected (as denoted by the brown or grey solid arrows), and further neighbours are disconnected (as denote by the grey dashed arrows). The position of each site in the studied fractal lattices can be mapped to the positions of the depicted central sites or their rotations, as the angles beside the pink circular regions indicate. The connectivity of a site is equal to the number of brown solid arrows, as indicated by the value of f. SG, Sierpiński gasket; SC, Sierpiński carpet; DSC, dual Sierpiński carpet.

where $|\Psi(0)\rangle$ is the initial state and $|\Psi(t)\rangle$ is the state at time t, and 'i' denotes the square root of -1. Since the longitudinal propagation length Z is proportional to the evolution time t (that is, $Z = vt$ where v is the speed of light in the medium), we can measure the evolution at different moments by preparing lattices of different lengths.

On the assumption of tight binding, only the evanescent coupling between the nearest-neighbour sites is taken into account. The Hamiltonian is thus generally expressed as

$$H = \sum_{i=1}^{N} \beta_i a_i^\dagger a_i + \sum_{(i,j)\in E} C_{i,j} a_i^\dagger a_j, \qquad (2)$$

where $a_i^\dagger$ and a_i are the creation and annihilation operators, respectively, for photons in site i, β_i is the propagation constant of site i, and $C_{i,j}$ is the coupling strength between the nearest-neighbour pair sites i and j, as denoted by the constraint $(i,j) \in E$, where E is the set composed of all the nearest-neighbour pairs of a lattice (see Methods). Therefore, the geometrical arrangement of a photonic lattice also has a notable influence on the Hamiltonian, leading to totally different quantum transport in different kinds of fractals, as we show below.

Besides the Sierpiński gasket, we investigate quantum transport in other fractals with different Hausdorff dimensions, namely the Sierpiński carpet and its transformation, the dual Sierpiński carpet, shown in Fig. 1d. The first-generation Sierpiński carpet, G(1), is produced by taking out the central part of a square, leaving eight blue squares, one of which is enclosed by the white dashed line. The higher generations are constructed through an iteration process and the corners of the blue squares in the Sierpiński carpet are defined as lattice sites. As for the dual Sierpiński carpet, its photonic lattice is constructed by replacing the blue squares in the second-generation Sierpiński carpet with lattice sites. Both the dual Sierpiński carpet and the Sierpiński carpet possess a fractal dimension of 1.89, which

is different from the Sierpiński gasket[34], but they have distinguishable geometric arrangements, such as the distribution of voids or lacunae (regions without lattice sites). The differences among these fractals allow us to study the influence on quantum transport not only of their fractal dimensions but also of their geometrical features.

We further analyse the connectivity of the fractal networks to identify their geometrical differences. Based on the tight-binding assumption, photon hopping only happens between the nearest-neighbour sites, as the solid (brown or grey) arrows in Fig. 1e indicate. Only these sites are mutually connected. Otherwise, they are disconnected, as denoted by the dashed arrows, owing to the fact that the distance between them is larger than the nearest-neighbour length (that is, the radius of the pink circular regions). In contrast to regular lattices, whose sites are connected by the nearest neighbours in all directions, in the fractal lattices some nearest sites are missing, therefore resulting in a diversity of connectivity and a lack of translational invariance, which to some degree introduces the 'geometric disorder'. Note that the position of each site in the studied fractal lattices can be mapped to either the position of the depicted central sites, or their rotations around the centre, as the angles on the top right sides of the pink regions indicate. The connectivity of the central sites in different positions is denoted by the value of f, which is equal to the number of brown arrows.

We collect the experimental evolution patterns on the three kinds of fractal photonic lattices with single input sites as presented in Figs. 2a, 3a and 4a, respectively. Selected experimental and simulated evolution patterns are exhibited in the left and right columns, respectively, of Figs. 2d, 3d and 4d, including those corresponding to the critical moments, which are highlighted with vertical dashed lines in Figs. 2b, 3b and 4b. The complete evolution patterns unveiling the quantum dynamics in full are shown in Supplementary Figs. 1–13. The MSD (shown in Figs. 2b, 3b and 4b) and the Pólya number (Figs. 2c, 3c and 4c) are presented in the plots, where the propagation length Z instead of time t acts as the evolution coordinate. Given that $Z=vt$, it makes no difference to use either of the two coordinates. The dynamic evolution and MSDs are shown in Supplementary Videos 1–3.

In the case of the Sierpiński gasket, the experimental and simulated MSDs exhibited in Fig. 2b have similar trends during the entire transport process. Besides the super-diffusive transport behaviour (that is, the MSD has a scaling exponent larger than 1)[45], we find that the scaling behaviour of the MSD is obviously changing, yielding a curve with a variational slope in a double-logarithmic plot, which is different from the constant quadratic growth in the case of infinite regular lattices[33,41]. This anomalous phenomenon indicates a transition in the transport behaviour of photons, and therefore implies a more complex regime of quantum transport in fractals than in regular media. It is also found that the fractal geometry determines the transition points of the transport. For instance, the first transition point, marked at the propagation length 2.675 mm, is exactly the critical point at which the photons reach the first void of the Sierpiński gasket, as the patterns in Fig. 2d reveal.

More details about the relation between the fractal geometry and the quantum-transport properties are revealed in the following. For simplicity, we use 'probe length', l_p, to roughly describe the transverse deviation of photons from the input site. In general, we define that l_p equals h when the photons reach the first void of the fractal. For $0<l_p<h$, corresponding to $0<Z<2.675$ mm, the evolution of photons follows the normal regime describing quantum transport in finite regular lattices (see Supplementary Fig. 14). However, the fractal geometry starts to come into play at the critical point $l_p=h$, or $Z=2.675$ mm. The photon transport behaviour gradually deviates from the normal regime with a decrease of the scaling exponent of the MSD until $l_p=l_f$ (the length at which the fractal regime starts to dominate), which is slightly larger than h and corresponds to $Z=3.875$ mm. As the green dashed line indicates, the subsequent evolution of photons is governed by an anomalous or fractal regime where the MSD is solely related to the fractal dimension d_f,

$$\langle r^2(t)\rangle \sim t^{d_f}, \tag{3}$$

which is radically different from the classical transport in fractals, where the MSD is governed by the ratio between the spectral dimension and the fractal dimension[27,28]. r is the displacement of the photons. We have further confirmed the robustness of the above relation by investigating quantum transport in large fractional space composed of thousands of lattice sites (see Supplementary Section 5) and by studying the influence of the input site's location on quantum transport (see Supplementary Section 6). Moreover, the fractal regime reported here coincides with the generalized description of quantum transport in lattices with fractal energy spectrum (see Methods), despite the fact that the fractality in the two cases is manifested differently[55]. The MSD keeps increasing, following the fractal regime, until photons get close to or reach the farthest site (corresponding to $Z=9.275$ mm). After that moment, the MSD exhibits saturation and small oscillations (see Methods).

The anomalies of the quantum transport are also experimentally and numerically observed in the Pólya number displayed in Fig. 2c. We magnify the plots highlighted with a hatched pattern for a clearer observation and show them in the insets. The evolution of the Pólya number undergoes a rapid growth at first and a subsequent plateau before 3.875 mm, which is the same as the Pólya number for the regular case (see Supplementary Fig. 17). However, we observe extra growth and plateaus, which appear alternately after 3.875 mm, as displayed in the inset. It should be noticed that the phenomenon does not appear in the regular cases and the propagation length 3.875 mm is exactly the starting point of the fractal regime, as shown in Fig. 2b, which corroborates the influence of the fractal geometry on the quantum transport.

In the case of the Sierpiński carpet, as demonstrated in Fig. 3b,c, the transport properties are qualitatively similar to the ones for the Sierpiński gasket, including the super-diffusive transport, the changing scaling behaviour of the MSD, the transition from the normal regime ($0<l_p<h$, $0<Z<3.85$ mm) to the fractal regime ($l_p>l_f$, $Z>5.95$ mm), the decisive role of the fractal dimension in the fractal regime and the emergence of extra growth and plateaus in the Pólya number. The only difference, the absence of saturation and oscillation of the MSD, owes to the fact that a much longer evolution time or propagation length of the photons is required to reach the farthest site of the lattice, which contains nearly 700 sites. The slight disagreement between the experiment and the simulation is due to inevitable imperfections in practical fabrications and realistic experimental environments, especially for such a large-scale lattice.

Distinctive to the above fractals, the fractal regime instead of the normal regime is probed at the very beginning of the quantum-transport process in the dual Sierpiński carpet. As Fig. 4b presents, both the experimental and simulated MSDs grow as $\sim Z^{1.89}$ in the fractal regime, when $Z<7.8$ mm (before the photons hit the farthest site, as shown in Fig. 4d). Subsequently, the MSD increases in a very slow manner and gradually saturates. In addition, weak oscillations emerge after the saturation. The disappearance of the normal regime is attributed to the fact that the void in the dual Sierpiński carpet is met from the very initial point and therefore the fractal geometry takes effect at early times. Meanwhile, as expected, a series of plateaus appear in the Pólya number from the beginning, as demonstrated in Fig. 4c. Though the dual Sierpiński carpet inherits the fractal dimension of the Sierpiński carpet, the transport dynamics in the two fractals have obviously distinguishable properties, reflecting that not only the fractal dimension but also other intrinsic features of the fractals play a crucial role in the quantum transport.

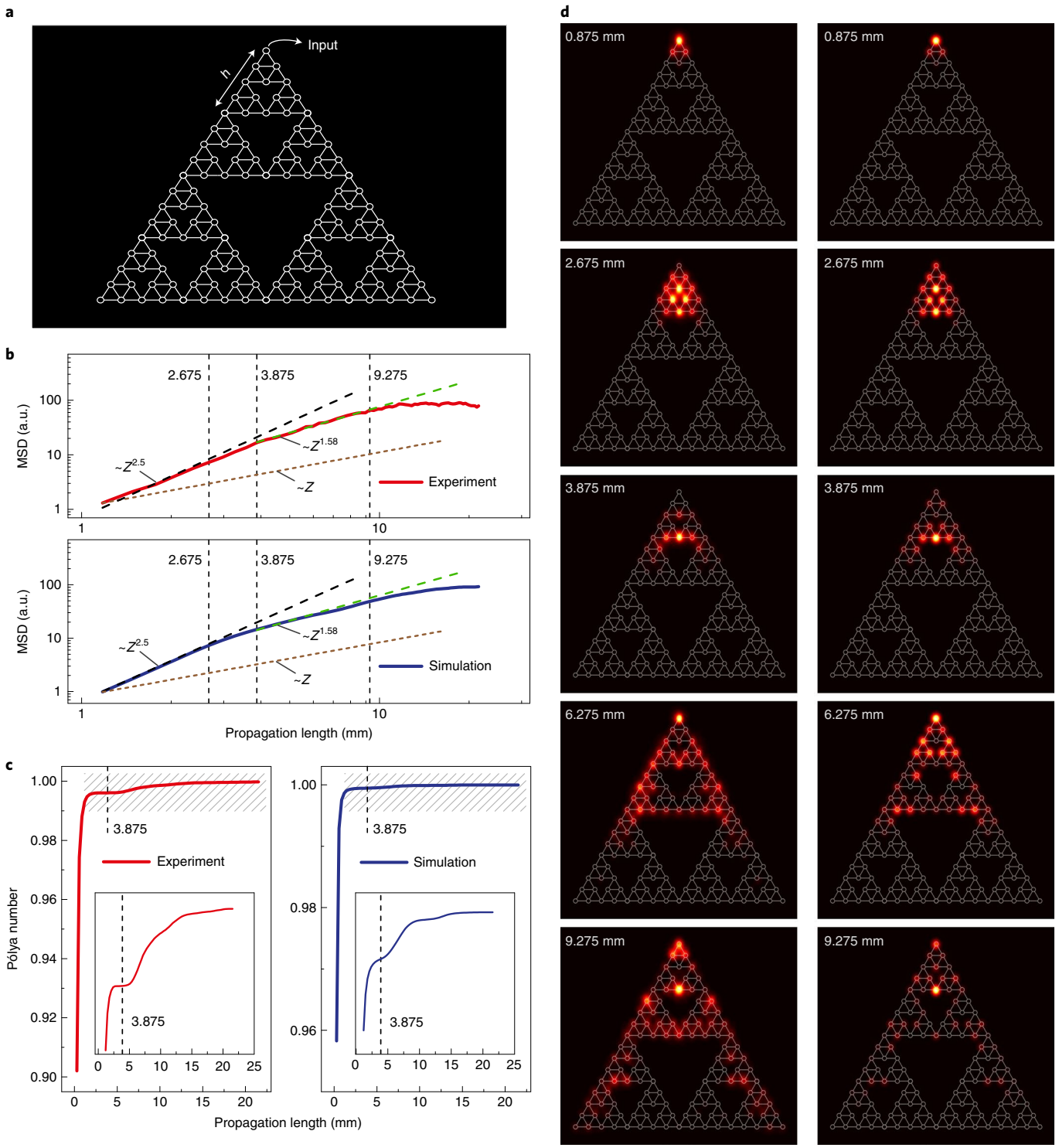

Fig. 2 | Quantum transport in the Sierpiński gasket. a, The photonic lattice for the fourth-generation Sierpiński gasket, with the apex as the input. The 'probe length' *h* describes the transverse deviation of photons when they reach the first void. **b**, The MSD shows different scaling behaviour, as the black and green dashed lines indicate. The transition points between different regimes are marked with vertical dashed lines. **c**, The Pólya number first grows rapidly, then reaches a plateau (before 3.875 mm). The plot highlighted by the hatched pattern is magnified and shown in the inset. Extra growth and plateaus appear after 3.875 mm. **d**, Experimental (left column) and simulated (right column) photon evolution patterns.

Discussion

In summary, we have investigated quantum transport in networks of non-integer dimension, including Sierpiński gaskets, Sierpiński carpets and dual Sierpiński carpets. With the implementation of continuous-time quantum walks in fractal photonic lattices, we revealed the transport process through either the direct observation of photon evolution patterns or the quantitative characterization based on the MSD and the Pólya number. In contrast to the classical counterpart, different transport properties are observed, confirming the non-classical feature of the transport, which is also manifested in the return probability (see Supplementary Fig. 16).

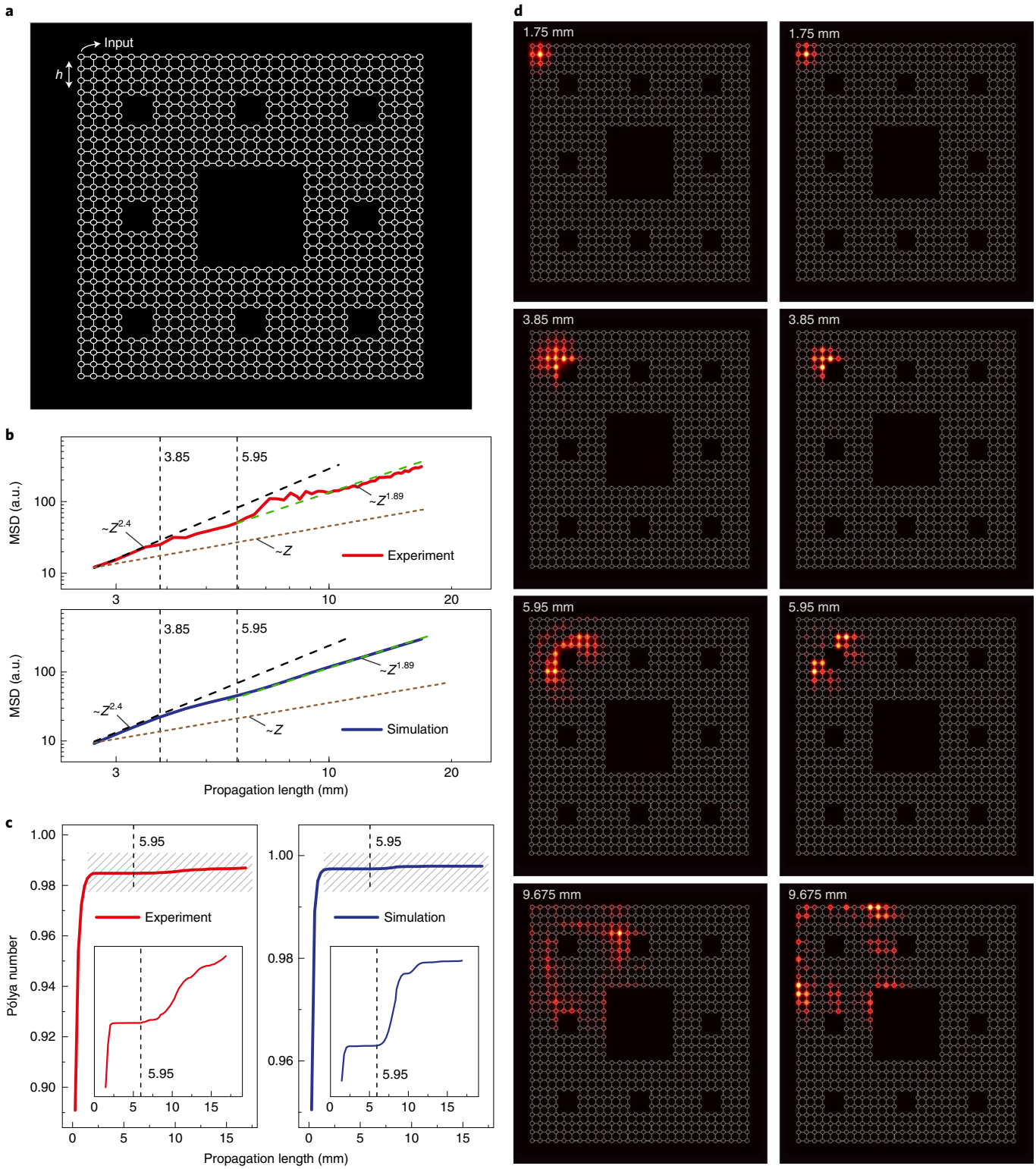

Fig. 3 | Quantum transport in the Sierpiński carpet. a, The photonic lattice for the third-generation Sierpiński carpet, with the top left corner as the input. The 'probe length' *h* describes the transverse deviation of photons when they reach the first void. **b**, The MSD shows different scaling behaviour, as the black and green dashed lines indicate. The transition points between different regimes are marked with vertical dashed lines. **c**, The Pólya number first increases rapidly, then reaches a plateau (before 5.95 mm). Extra growth and plateaus are found after 5.95 mm, as shown in the inset (the magnification of the plot highlighted by the hatched pattern). **d**, Experimental (left column) and simulated (right column) photon evolution patterns.

Compared with infinite regular lattices, the quantum transport in fractals is anomalous. First, the transport dynamics cannot be simply described by a single regime. Here, we find a crossover from the normal to the fractal regime in the cases of the Sierpiński gasket and the Sierpiński carpet, which is revealed by a change in the scaling behaviour of the MSD and by the extra growth and plateaus in

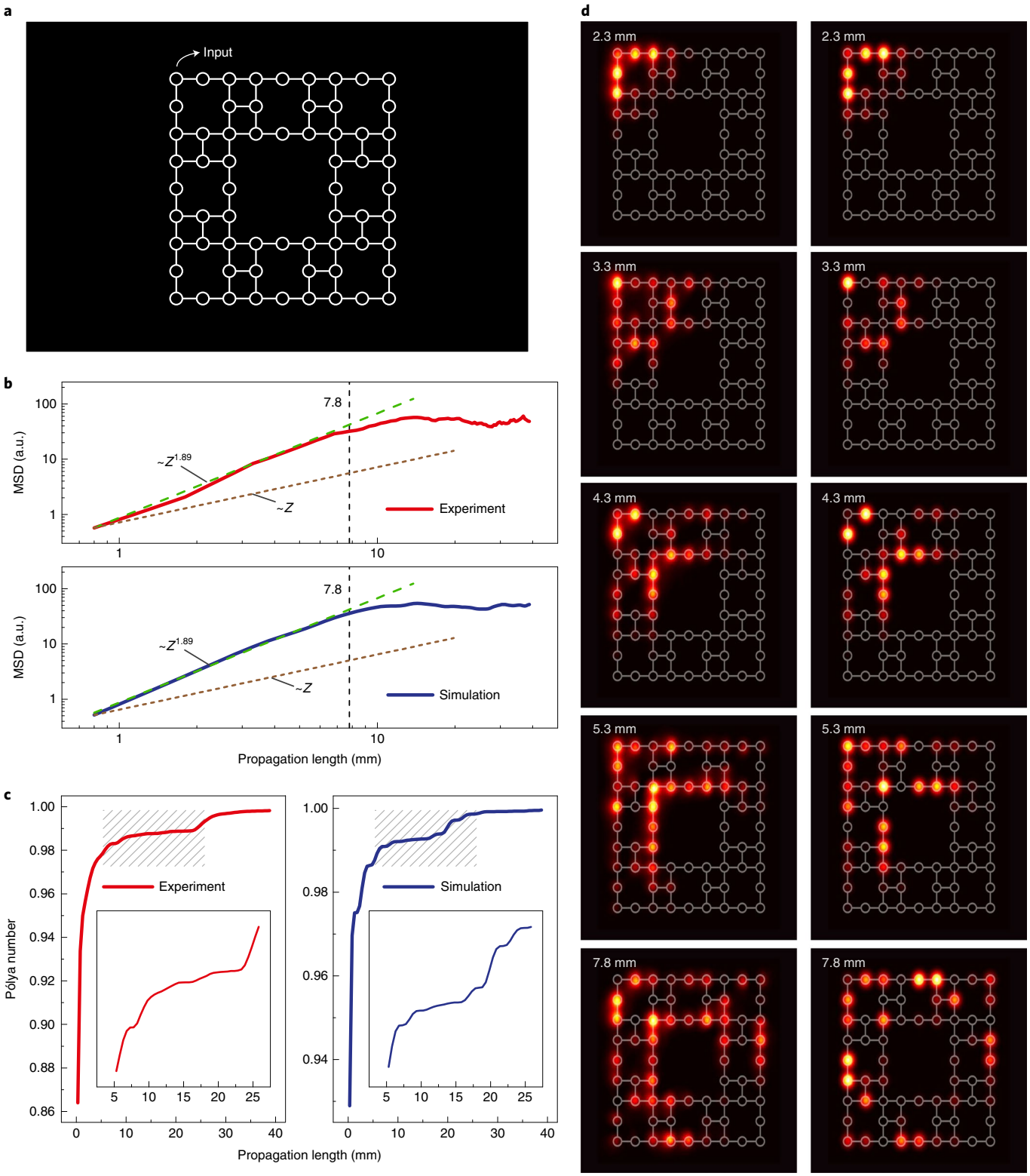

Fig. 4 | Quantum transport in the dual Sierpiński carpet. a, The photonic lattice for the dual Sierpiński carpet, a transformation of the second-generation Sierpiński carpet, with the top left corner as the input. **b**, The MSD first grows as $\sim Z^{1.89}$ (as the green dashed line suggests). Then, it slowly increases and gradually saturates. The transition point is marked with vertical dashed lines. **c**, The Pólya number undergoes a series of growing stages and plateaus from the very beginning. The part of the plot highlighted with a hatched pattern is magnified and shown in the inset. **d**, Experimental (left column) and simulated (right column) photon evolution patterns.

the Pólya number (after the first plateau). Second, the fractal features of the network play an important role in quantum transport. Indeed, the evolution of the MSD in the fractal regime is completely determined by the fractal dimension. Last but not least, the transport dynamics are also closely related to the geometrical features of the fractals. For one thing, the normal regime disappears in the case

of the dual Sierpiński carpet, but not in the case of the Sierpiński carpet, though they have the same fractal dimension. For another, the transition points between the different regimes correspond to the moments when the photons reach particular positions of the fractal lattices, such as the first void and the farthest site.

Our work sets the stage for the understanding of quantum transport in several disciplines. Given the fractal nature of organisms, for example, trees and human bodies[10], it might shed some light on whether or not quantum mechanics plays any role in the transport in biological systems. The orchestrated objective reduction (Orch OR) theory proposed that consciousness originates from microtubules inside neurons, where quantum coherence emerges, and that consciousness may occur at various scales in a fractal-like brain hierarchy[56,57]. The theory generated much controversy, with strong opponents and persuaded supporters, but the issue has not been settled. Whatever conclusion to emerge might profit from the experiments performed here. In addition, our results may also contribute to the understanding of quantum transport in disordered systems, since fractals are a good model for most disordered media[25,58]. Finally, our experimental demonstrations lay a strong foundation for the implementation of the quantum Grover search algorithm in fractals[59]. The anomalous quantum dynamics reported here may provide new degrees of freedom for the design of quantum algorithms based on quantum walks. Therefore, by investigating quantum transport in artificially designed fractal structures, we might be making the first steps towards the long journey that will be the unification of physics, mathematics, biology and computer science, to reach a deeper understanding of the human body and its functioning, as well as to inspire designs of more efficient quantum algorithms.

Online content

Any methods, additional references, Nature Research reporting summaries, source data, extended data, supplementary information, acknowledgements, peer review information; details of author contributions and competing interests; and statements of data and code availability are available at https://doi.org/10.1038/s41566-021-00845-4.

Received: 9 October 2020; Accepted: 13 June 2021;
Published online: 19 July 2021

References

1. Mandelbrot, B. B. *Fractals: Form, Chance and Dimension* (W. H. Freeman, 1977).
2. ben-Avraham, D. & Havlin, S. *Diffusion and Reactions in Fractals and Disordered Systems* (Cambridge Univ. Press, 2000).
3. Mandelbrot, B. B. *The Fractal Geometry of Nature* (W. H. Freeman, 1983).
4. Gouyet, J.-F. *Physics and Fractal Structures* (Springer, 1996).
5. Ivanov, P. C. et al. Multifractality in human heartbeat dynamics. *Nature* **399**, 461–465 (1999).
6. Bandres, M. A., Rechtsman, M. C. & Segev, M. Topological photonic quasicrystals: fractal topological spectrum and protected transport. *Phys. Rev. X* **6**, 011016 (2016).
7. Tanese, D. et al. Fractal energy spectrum of a polariton gas in a Fibonacci quasiperiodic potential. *Phys. Rev. Lett.* **112**, 146404 (2014).
8. Hofstadter, D. R. Energy levels and wave functions of Bloch electrons in rational and irrational magnetic fields. *Phys. Rev. B* **14**, 2239–2249 (1976).
9. Brady, R. & Ball, R. Fractal growth of copper electrodeposits. *Nature* **309**, 225–229 (1984).
10. Goldberger, A. L. et al. Fractal dynamics in physiology: alternations with disease and aging. *Proc. Natl Acad. Sci. USA* **99**, 2466–2472 (2002).
11. Bassingthwaighte, J. B., Liebovitch, L. S. & West, B. J. *Fractal Physiology* (Springer, 2013).
12. Peters, E. E. Fractal structure in the capital markets. *Financ. Anal. J.* **45**, 32–37 (1989).
13. Dean, C. R. et al. Hofstadteras butterfly and the fractal quantum Hall effect in moiré superlattices. *Nature* **497**, 598–602 (2013).
14. Wang, L. et al. Evidence for a fractional fractal quantum Hall effect in graphene superlattices. *Science* **350**, 1231–1234 (2015).
15. Benedetti, D. Fractal properties of quantum spacetime. *Phys. Rev. Lett.* **102**, 111303 (2009).
16. Karman, G., McDonald, G., New, G. & Woerdman, J. Fractal modes in unstable resonators. *Nature* **402**, 138 (1999).
17. Dudley, J. M., Finot, C., Richardson, D. J. & Millot, G. Self-similarity in ultrafast nonlinear optics. *Nat. Phys.* **3**, 597–603 (2007).
18. Rivera, J. A., Galvin, T. C., Steinforth, A. W. & Eden, J. G. Fractal modes and multi-beam generation from hybrid microlaser resonators. *Nat. Commun.* **9**, 2594 (2018).
19. Ding, J., Fan, L., Zhang, S.-Y., Zhang, H. & Yu, W.-W. Simultaneous realization of slow and fast acoustic waves using a fractal structure of Koch curve. *Sci. Rep.* **8**, 1481 (2018).
20. Fan, J. A. et al. Fractal design concepts for stretchable electronics. *Nat. Commun.* **5**, 3266 (2014).
21. Fazio, B. et al. Strongly enhanced light trapping in a two-dimensional silicon nanowire random fractal array. *Light Sci. Appl.* **5**, e16062 (2016).
22. Gottheim, S., Zhang, H., Govorov, A. O. & Halas, N. J. Fractal nanoparticle plasmonics: the Cayley tree. *ACS Nano* **9**, 3284–3292 (2015).
23. De Nicola, F. et al. Multiband plasmonic Sierpinski carpet fractal antennas. *ACS Photonics* **5**, 2418–2425 (2018).
24. Zhu, L.-H. et al. Broadband absorption and efficiency enhancement of an ultra-thin silicon solar cell with a plasmonic fractal. *Opt. Express* **21**, A313–A323 (2013).
25. Havlin, S. & Ben-Avraham, D. Diffusion in disordered media. *Adv. Phys.* **36**, 695–798 (1987).
26. Blumen, A., Klafter, J., White, B. & Zumofen, G. Continuous-time random walks on fractals. *Phys. Rev. Lett.* **53**, 1301 (1984).
27. Alexander, S. & Orbach, R. Density of states on fractals: fractons. *J. Phys. Lett.* **43**, 625–631 (1982).
28. Orbach, R. Dynamics of fractal networks. *Science* **231**, 814–819 (1986).
29. Ben-Avraham, D. & Havlin, S. Diffusion on percolation clusters at criticality. *J. Phys. A Math. Gen.* **15**, L691 (1982).
30. Sokolov, I. M. What is the alternative to the Alexander–Orbach relation? *J. Phys. A Math. Theor.* **49**, 095003 (2016).
31. Reis, F. D. A. & Voller, V. R. Models of infiltration into homogeneous and fractal porous media with localized sources. *Phys. Rev. E* **99**, 042111 (2019).
32. Mülken, O. & Blumen, A. Continuous-time quantum walks: models for coherent transport on complex networks. *Phys. Rep.* **502**, 37–87 (2011).
33. Agliari, E., Blumen, A. & Mülken, O. Dynamics of continuous-time quantum walks in restricted geometries. *J. Phys. A Math. Theor.* **41**, 445301 (2008).
34. Darázs, Z., Anishchenko, A., Kiss, T., Blumen, A. & Mülken, O. Transport properties of continuous-time quantum walks on Sierpinski fractals. *Phys. Rev. E* **90**, 032113 (2014).
35. Volta, A. Quantum walks and trapping on regular hyperbranched fractals. *J. Phys. A Math. Theor.* **42**, 225003 (2009).
36. van Veen, E., Yuan, S., Katsnelson, M. I., Polini, M. & Tomadin, A. Quantum transport in Sierpinski carpets. *Phys. Rev. B* **93**, 115428 (2016).
37. Feng, Z. et al. Photonic Newton's cradle for remote energy transport. *Phys. Rev. Appl.* **11**, 044009 (2019).
38. Tang, H. et al. Experimental quantum fast hitting on hexagonal graphs. *Nat. Photonics* **12**, 754–758 (2018).
39. Perets, H. B. et al. Realization of quantum walks with negligible decoherence in waveguide lattices. *Phys. Rev. Lett.* **100**, 170506 (2008).
40. Peruzzo, A. et al. Quantum walks of correlated photons. *Science* **329**, 1500–1503 (2010).
41. Tang, H. et al. Experimental two-dimensional quantum walk on a photonic chip. *Sci. Adv.* **4**, eaat3174 (2018).
42. Schwartz, T., Bartal, G., Fishman, S. & Segev, M. Transport and Anderson localization in disordered two-dimensional photonic lattices. *Nature* **446**, 52–55 (2007).
43. Lahini, Y. et al. Anderson localization and nonlinearity in one-dimensional disordered photonic lattices. *Phys. Rev. Lett.* **100**, 013906 (2008).
44. Segev, M., Silberberg, Y. & Christodoulides, D. N. Anderson localization of light. *Nat. Photonics* **7**, 197–204 (2013).
45. Naether, U. et al. Experimental observation of superdiffusive transport in random dimer lattices. *New J. Phys.* **15**, 013045 (2013).
46. Eichelkraut, T. et al. Mobility transition from ballistic to diffusive transport in non-Hermitian lattices. *Nat. Commun.* **4**, 2533 (2013).
47. Shang, J. et al. Assembling molecular Sierpiński triangle fractals. *Nat. Chem.* **7**, 389–393 (2015).
48. Newkome, G. R. et al. Nanoassembly of a fractal polymer: a molecular 'Sierpinski hexagonal gasket'. *Science* **312**, 1782–1785 (2006).
49. Rothemund, P. W., Papadakis, N. & Winfree, E. Algorithmic self-assembly of DNA Sierpinski triangles. *PLoS Biol.* **2**, e424 (2004).
50. Kempkes, S. N. et al. Design and characterization of electrons in a fractal geometry. *Nat. Phys.* **15**, 127–131 (2019).
51. Jia, S. & Fleischer, J. W. Nonlinear light propagation in fractal waveguide arrays. *Opt. Express* **18**, 14409–14415 (2010).

52. Osellame, R., Cerullo, G. & Ramponi, R. (eds) *Femtosecond Laser Micromachining: Photonic and Microfluidic Devices in Transparent Materials* Vol. 123 (Springer, 2012).
53. Xu, X.-Y. et al. A scalable photonic computer solving the subset sum problem. *Sci. Adv.* **6**, eaay5853 (2020).
54. Darázs, Z. & Kiss, T. Pólya number of the continuous-time quantum walks. *Phys. Rev. A* **81**, 062319 (2010).
55. Fleischmann, R., Geisel, T., Ketzmerick, R. & Petschel, G. Quantum diffusion, fractal spectra, and chaos in semiconductor microstructures. *Physica D* **86**, 171–181 (1995).
56. Hameroff, S. & Penrose, R. Consciousness in the universe: a review of the 'Orch OR' theory. *Phys. Life Rev.* **11**, 39–78 (2014).
57. Hameroff, S. & Penrose, R. Orchestrated reduction of quantum coherence in brain microtubules: a model for consciousness. *Math. Comput. Simul.* **40**, 453–480 (1996).
58. Gefen, Y., Aharony, A., Mandelbrot, B. B. & Kirkpatrick, S. Solvable fractal family, and its possible relation to the backbone at percolation. *Phys. Rev. Lett.* **47**, 1771 (1981).
59. Agliari, E., Blumen, A. & Mülken, O. Quantum-walk approach to searching on fractal structures. *Phys. Rev. A* **82**, 012305 (2010).

Methods

Preparation of fractal photonic lattices. The fractal photonic lattices are produced by skipping over the writing of particular sites in the regular lattices corresponding to the fractals. Note that the regular lattices are constructed by filling the voids in the fractals with lattice sites. For example, the lattice for the dual Sierpiński carpet or the Sierpiński carpet corresponds to a square lattice with the same size. Before fabrication, based on the iterative rule for each fractal, an extra programme is used to generate a matrix whose element is either 1 or 0 to control whether a site should be written or not. Then, the matrix is imported into the fabrication programme that is originally designed for the regular lattices. Under the external control of the matrix and with the translational stage moving at a constant velocity of 10 mm s^{-1}, the lattices with a desirable fractal geometry are successfully fabricated using the femtosecond laser (a repetition rate of 1 MHz, a central wavelength of 513 nm and a pulse duration of 290 fs) focused by a ×50 object. Laser beam shaping through a spatial light modulator and depth-dependent pulse energy compensation are applied to obtain uniform lattices.

The Hamiltonian of fractal photonic lattices. In a uniform lattice, the propagation constant for each site is equal (that is, $\beta_i = \beta$, $i = 1,2,...,N$). Since the coupling coefficient is direction-dependent, the site spacings are properly selected to ensure the same coupling coefficients for all the nearest-neighbour pairs (that is, $C_{ij} = C$, $(i,j) \in E$), as done in our previous research[41]. Similar to the fabrication procedure, the Hamiltonian of fractal photonic lattices is constructed from the Hamiltonian of their corresponding regular lattices. The specific procedure is described as follows. First of all, we uniquely index each site in the regular lattices. For a lattice containing N sites, an $N \times N$ Hamiltonian matrix is acquired. Second, all the diagonal elements of the Hamiltonian are set as β. Besides, based on the geometry of the regular lattices and tight-binding assumption, the non-diagonal elements are set to be either C or zero. Last, according to the iterative rule of the fractals, the sites located in the region corresponding to the voids in the fractals are picked out and then all the coupling coefficients related to these sites are set as zero to obtain the Hamiltonian for the fractals.

Simulation of photon evolution. The simulated results of photon evolution are obtained by solving equation (1). For a lattice containing N sites, the state localized at site j is represented by $|j\rangle$, and the states $\{|j\rangle, j = 1,2,...,N\}$ provide an orthonormal basis set[33]. Therefore, the system state at time t can be written as $|(t)\rangle = \sum_{j=1}^{N} a_j(t)\,|j\rangle$, where $|a_j(t)|^2 = p_j(t)$, that is, the probability of photons being found at site j at time t. In our case, only one site is initially excited (that is, there is only one input for photons) and therefore the initial state is denoted as $|\Psi(0)\rangle = |1\rangle$. As a consequence, equation (1) can be expressed as

$$\sum_{j=1}^{N} a_j(t)\,|j\rangle = \mathrm{e}^{-iHt}\,|1\rangle\,. \tag{4}$$

Then we find that $|a_j(t)|^2 = |\langle j|U(t)|1\rangle|^2 = |U_{j,1}(t)|^2$, where the time evolution operator $U(t) = \mathrm{e}^{-iHt}$. Based on the Hamiltonian of the system, we calculate $U(t)$ through a Python function to obtain the probability of photons being found at each site and then display it in the form of Gaussian spots.

The fractal regime of quantum transport. As proposed by the theoretical research[55], in the case of lattices with fractal energy spectrum, the MSD is generalized as

$$\left\langle r^2(t) \right\rangle \sim t^{2d_f/D}, \tag{5}$$

where D is the Euclidean dimension in which the lattice is embedded. For a lattice embedded in two-dimensional space, equation (5) can be written as $\left\langle r^2(t) \right\rangle \sim t^{d_f}$, which is the same as the fractal regime in our case, where the lattices show fractality in geometry.

The saturation and oscillation of the mean square displacement. The definition of the MSD is given by the equation

$$\left\langle r^2(t) \right\rangle = \sum_{j=1}^{N} r_j^2 p_j(t), \tag{6}$$

where r_j is the normalized distance between the input site and site j. The MSD is determined by the transverse deviation and the probability distribution of the photons. As photons transversely travel farther, the MSD becomes larger. Meanwhile, when it is more possible to find a photon at sites far from the input, the MSD tends to be larger. Therefore, as long as photons spread towards the farthest place, the MSD keeps growing. The growth holds even when photons encounter the voids of the fractals, because the forward spreading is not completely stopped by the voids, though it is indeed slowed down. However, once the farthest site is reached or almost reached, the MSD starts to increase very slowly and then gradually saturates. It is the finite size of the lattices that makes the saturation inevitable. The appearance of small oscillations could be a result of the complex interaction among the forward wave, the reflected wave from the farthest site and from the voids scattered across the fractals, which is still an open problem and might require further investigations.

Data availability

The data that support the findings of this study are available from the corresponding authors on reasonable request.

Acknowledgements

We thank J.-W. Pan for helpful discussions, X.-L. Huang and Z.-M. Li for helping in the experiments, J. Gao, R.-J. Ren and S. Freeney for proof reading, and W.-H. Zhou for assistance in formatting the figures. This research is supported by the National Key R&D Program of China (2019YFA0308700, 2019YFA0706302 and 2017YFA0303700); National Natural Science Foundation of China (NSFC) (11904229, 61734005, 11761141014, 11690033); Science and Technology Commission of Shanghai Municipality (STCSM) (20JC1416300, 2019SHZDZX01); Shanghai Municipal Education Commission (SMEC) (2017-01-07-00-02-E00049); China Postdoctoral Science Foundation (2021M692094, 2020M671091). X.-M.J. acknowledges additional support from a Shanghai talent program and support from Zhiyuan Innovative Research Center of Shanghai Jiao Tong University.

Author contributions

X.-M.J. conceived and supervised the project. X.-Y.X. performed the simulations and fabricated the photonic chips. X.-Y.X., X.-W.W., D.-Y.C. and X.-M.J. performed the experiments and analysed the data. X.-Y.X., C.M.S. and X.-M.J. interpreted the data and wrote the paper, with input from all the other authors.

Competing interests

The authors declare no competing interests.

Additional information

Supplementary information The online version contains supplementary material available at https://doi.org/10.1038/s41566-021-00845-4.

Correspondence and requests for materials should be addressed to C.M.S. or X.-M.J.

Peer review information *Nature Photonics* thanks Eric Heller and Shengjun Yuan for their contribution to the peer review of this work.